In operando simultaneous ATR-IR/Raman spectroscopic investigation of the catalytic activity of supported Pt, Ru, and Pd catalysts in H/D exchange reactions between H2 and D2O

Isaline Bonnin, Raphaël Mereau, Karine de Oliveira Vigier, Thierry Tassaing

In operando simultaneous ATR-IR/Raman spectroscopic investigation of the catalytic activity of supported Pt, Ru, and Pd catalysts in H/D exchange reactions between H_2 and D_2O.

Isaline Bonnin[1,2], Raphaël Mereau[1], Karine De Oliveira Vigier[2], Thierry Tassaing[1]*

[1] Institut des Sciences Moléculaires (ISM), Univ. Bordeaux, CNRS, Bordeaux INP, ISM, UMR 5255, F-33400 Talence, France

[2] Institut de Chimie des Milieux et Matériaux de Poitiers (IC2MP), Univ. de Poitiers, UMR CNRS 7285, 1 rue Marcel Doré, 86073 Poitiers Cedex 9, France

Corresponding author: thierry.tassaing@u-bordeaux.fr

Abstract

In this study, catalytic H/D exchange experiments have been performed between H_2 and D_2O catalyzed by supported metal catalysts, namely, Ru/Al_2O_3, Pt/Al_2O_3 and Pd/Al_2O_3 in order to unveil the reaction mechanism at work in the glucose hydrogenation reaction on these supported metal catalysts. The conversion of H_2 and D_2O towards the formation of the exchange species namely HOD, HD and D_2 was investigated using *in operando* simultaneous ATR-IR/Raman spectroscopy allowing the monitoring of the liquid/gas phase respectively. After 24 h of reaction at 22 °C under 30 bar of H_2, it is found that Pt/Al_2O_3 has the highest efficiency for the H/D exchange between H_2 and D_2O, followed by Ru/Al_2O_3 and then Pd/Al_2O_3. On the other hand, the enhanced activity of Ru/Al_2O_3 for the hydrogenation of glucose is tentatively assigned to H atoms adsorbed and activated on the Ru surface leading to an Ru-H infrared band located around 1940-1970 cm^{-1}, that is observed only with Ru/Al_2O_3. This activated H* could be directly added to the carbon atom of the carbonyl of glucose to give sorbitol in a more efficient way compared to the other metals.

Keywords: Isotopic Exchange, Deuterated water, Dihydrogen, Hydrogenation, Glucose, Ruthenium, Platinum, Palladium, *In operando* spectroscopy

Introduction

Due to the use of lignocellulosic biomass as raw material, more and more catalytic reaction are performed in water. Hence, water allows the dissolution of carbohydrates contained in lignocellulosic biomass. An important reaction starting from sugars is the hydrogenation of sugars to sugar alcohol. For instance, sorbitol is a commodity chemical produced with high tonnage for paper industry, food and cosmetic applications. As sorbitol can be obtained from glucose hydrogenation (**Fig. 1**), contained in the carbohydrate part of lignocellulose, it was identified in 2004 by the US Department of Energy as one of the building blocks materials to high-value bio-based chemicals [1]. During this reaction, it is of prime interest to understand the exact role of water on the catalyst.

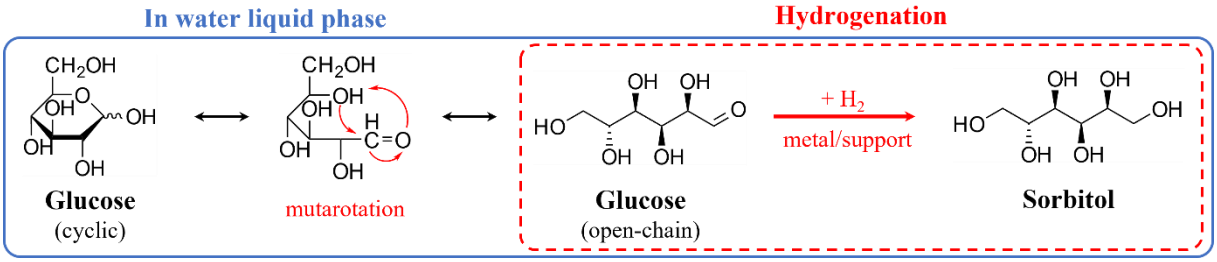

Figure 1: Hydrogenation of glucose to sorbitol catalyzed by a metal catalyst in aqueous liquid phase.

The synthesis of sorbitol from glucose is mostly performed with Raney-type nickel catalysts or nickel supported catalysts due to its high hydrogenation activity [2–8]. However, due to the leaching of nickel, the study of more stable, selective and active catalysts was carried out. Ru catalyst was found as the best alternative for the selective hydrogenation of glucose to sorbitol in comparison to Pt or Pd noble metals [9–11]. Indeed, in a recent work, we have demonstrated that a commercial catalyst Ru/Al_2O_3 was very active and selective for the hydrogenation of glucose to sorbitol in comparison to Pt/Al_2O_3 and Pd/Al_2O_3 that were found to be inactive for this reaction (**Table 1**) [11]. The conversion and yield without catalyst that is found higher than that with Pd or Pt as catalyst could be related to thermal degradation of glucose into humins while the addition of catalyst Pd/Al_2O_3 and Pt/Al_2O_3 probably limits this side reaction.

Table 1: Screening of commercial metal catalysts (5 wt.% of metal, average particle size of 2 nm) for the hydrogenation of glucose in aqueous liquid phase under 30 bar of H_2 at 120 °C for 1 h [11].

	Glucose conversion (%)	Sorbitol yield (%)
No catalyst	16	2
Pd	2	1
Pt	7	1
Ru	100	80

Beyond the hydrogenation of glucose, the detailed review of Besson *et al.* emphasizes that Ru catalysts are also very efficient for the hydrogenation of various aldoses and carboxylic derivatives such as arabinose, galactose, rhamnose, levulinic acid or succinic acid [10]. According to the literature, such activity is related to the presence of water that, on the one hand, stabilizes intermediates adsorbed on Ru metal surface by solvation effect [12,13] and, on the other hand, directly plays a catalytic role in the hydrogenation mechanism [14].

Investigated computationally [14–21] and experimentally [22–24], the hydrogenation mechanism in the liquid aqueous phase is likely to proceed through a catalytic exchange between an adsorbed H (H*) from H_2 and water. As the H* from H_2 is transferred to water molecule, it suggests that the replacement of H_2O by D_2O, or gaseous H_2 with D_2, allows to follow the exchange of protons that occurs at the solid-liquid interface. Thus, to investigate the catalytic exchange of H^* to water at the metal-liquid interface, few research works have reported the influence of metal for the production of exchange species HOD when water is replaced by deuterated water [25–27]. In particular, exchange species like HOD, HD and D_2 were detected for independent gas and aqueous phase investigations for the hydrodeoxygenation of guaiacol

over Ni/Nb_2O_5 putting in evidence the D_2O-H_2 exchange involvement in the mechanism [21]. Analysis of the aqueous phase by infrared spectroscopy have proven the formation of HOD and a production of HD and D_2 was detected in the gas phase by mass spectrometry. Others have studied the conversion of cinnamaldehyde into cinnamyl alcohol over Pt_3Fe and suggest that water participated in the catalytic hydrogenation reaction by serving as a hydrogen-exchange bridge [17].

In this context, we perform similar experiments in order to get insights into the mechanistic aspects of the hydrogenation of glucose to sorbitol in water over the supported metal catalyst Ru/Al_2O_3, Pt/Al_2O_3 and Pd/Al_2O_3 that were used in our previous study [11]. The main aim was to explain the high activity of Ru/Al_2O_3 in comparison to Pt/Al_2O_3 and Pd/Al_2O_3 (**Table 1**). To this aim, we have performed some *in operando* experiments on H_2/D_2O mixtures under high pressure at different temperatures in the presence of the supported metal catalysts cited above in order to compare their ability to perform the catalytic isotopic exchange between H_2 and D_2O. To monitor the exchange species as HOD, HD and D_2, we have designed an innovative *in operando* spectroscopic method using a single high-pressure cell for the simultaneous coupling of ATR-IR and Raman spectroscopy allowing the monitoring of the liquid and gas phase respectively. Moreover, the H/D exchange was also followed using the same methodology during the hydrogenation of glucose to sorbitol over Ru/Al_2O_3 catalyst.

Materials and methods

1. Materials

H_2 and D_2O were used as received with the following characteristics: H_2 (Air Liquid, 99.9999 %), D_2O (CEA saclay, 99.9 % purity). The catalysts Pd/Al_2O_3, Pd/Al_2O_3 and Ru/Al_2O_3 were purchased from Alfa Aeser. The metal content and the average particles sizes of catalysts were measured by ICP-OES (Inductively Coupled Plasma Optical Emission Spectrometry) and TEM (Transmission Electronic Microscopy). Catalysts exhibit a similar metal content (4.3 wt. % for Pd, 5.3 wt. % for Pt and 4.7 wt. %for Ru) and a similar average particle size (2 nm) allowing a proper comparison of these materials for the H/D exchange experiments. Especially, XRD analysis of Ru/Al_2O_3 have shown that the support is composed of a mixture of alumina phases identified as aluminium oxide (Al_2O_3) with a monoclinic crystalline structure (JCPDS 98-006-6560) and gamma alumina (γ-Al_2O_3) with tetragonal (JCPDS 98-009-9836) and cubic crystalline phases (JCPDS 10-1425).

2. High pressure simultaneous operando ATR-IR/Raman spectroscopy

2.1. High pressure cell

The monitoring of the catalytic H/D exchange by simultaneous operando ATR-IR/Raman spectroscopy is performed in a single high-pressure cell (**Fig. 2** and **Fig. S1 in ESI 1**). The cell has two parts, an ATR-FTIR part located at the bottom for liquid phase measurements and the other located at the top is the Raman cell for gas phase analysis.

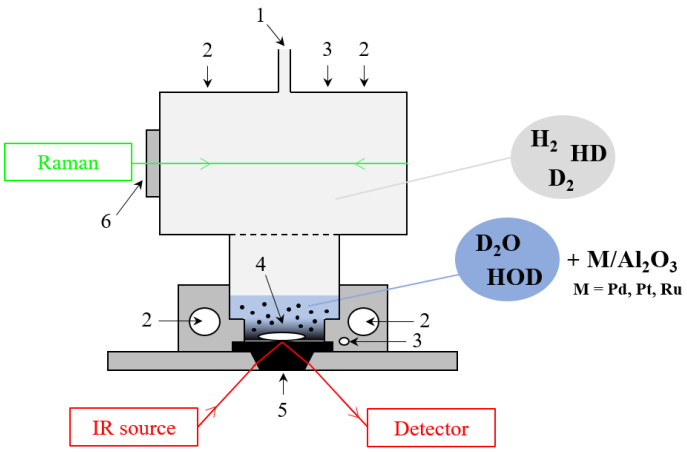

Figure 2: High-pressure experimental device with a single cell coupled with ATR-FTIR and Raman spectrometers for *in operando* simultaneous measurements of the catalytic H/D exchange of D_2O and H_2 producing HOD, HD and D_2 (1: gas/liquid entrance, 2: cartridges heaters, 3: thermocouple, 4: stirrer, 5: silicon crystal, 6: sapphire window).

The ATR part is composed of a silicon crystal to measure the wavelength range between 1000 $cm^{-1}$and 4000 cm^{-1}. The crystal has a visible surface of 50 mm^2 and it resists to high pressure thanks to its T-shape that allows blocking and sealing the crystal between two layers of the ATR accessory by the unsupported area principle. The ATR part of the cell is connected to the upper part of the cell composed of a sapphire window for Raman scattering. For a homogeneous temperature, the two parts of the cell can be heated independently using two cartridges' heaters each side of the ATR part and two cartridges' heaters disposed behind the Raman cell with thermocouples for each couple of cartridges to regulate the temperature with the accuracy of about $\Delta T = \pm 0.5$ °C. At the top of the Raman cell, a stainless capillary is connected to gas H_2 and to a pressure sensor with an accuracy of about $\Delta P = \pm 0.1$ bar. To ensure a good mixing of the liquid phase, a stirrer is deposited on the ATR crystal and a magnetic plate is put next to the cell. The total volume of the cell is 5 cm^3 and to ensure the sealing between the two parts, flat Kapton® rings are used between plugs and the high-pressure cell body.

2.2. Infrared/Raman set-up

For the ATR-IR measurements, a Nicolet 6700 FTIR spectrometer equipped with a Globar source, a KBr/Ge beamsplitter and a DLaTGS/KBr thermal detector was used to investigate the spectral range from 400 to 4000 cm^{-1}. Single beam spectra with 4 cm^{-1} resolution are obtained by Fourier transformation of 100 accumulated interferograms in order to improve the signal-to-noise ratio.

For IR absorption measurements, a Nicolet 6700 FTIR spectrometer equipped with a Globar source, a KBr/Ge beamsplitter and a DLaTGS/KBr thermal detector was used to investigate the spectral range from 400 to 6500 cm^{-1}. Single beam spectra with 4 cm^{-1} resolution are obtained by Fourier transformation of 100 accumulated interferograms in order to improve the signal-to-noise ratio.

2.3. Experimental procedure

For a typical catalytic H/D exchange experiment, 10 mg of catalyst M/Al_2O_3 is deposited on the ATR crystal. Then, the Raman part is connected to the ATR part and.an excess of D_2O (300 µL, 1.66 10^{-2} mol) is injected with a syringe from the upper part to the ATR crystal where a magnetic stirrer constantly homogenizes the liquid during the experiment. Prior to the introduction of 30 bar of H_2 at ambient temperature or 37 bar of H_2 at 90 °C (that corresponds to 5.95 10^{-3} mol of H_2 according to the NIST database [28]), acquisitions of both ATR-FTIR and Raman spectra are started at the same time to get a concomitant monitoring of D_2O, HOD, H_2, HD and D_2 during 24 h. During the experiment, infrared acquisitions of 210 s are recorded continuously for 24 h for the monitoring of D_2O and HOD species. Stretch and bending bands of D_2O and HOD at 1205 cm^{-1} (D-O-D bending), 1456 cm^{-1} (H-O-D bending) and 3401 cm^{-1} (O-H stretch) are chosen for further kinetics analysis by using baseline integration from 1800 to 1330 cm^{-1} for D-O-D and H-O-D vibrations and from 3780 to 3050 cm^{-1} for O-H vibration. Regarding the Raman spectra, one background of the empty high-pressure cell is recorded after 1 scan of 15 seconds of time integration and no other background is performed during the experiment. During the experiment, an acquisition of 30 s of the gas phase for the monitoring of H_2, HD and D_2 is executed and re-executed after 270 s and this loop of acquisitions lasts during the whole experiment of 24 h. The rotational band of H_2 at 580 cm^{-1} is integrated from 720 to 490 cm^{-1} for kinetic profiles. Vibrons of H_2 at 4160 cm^{-1} is integrated from 4256 to 4070 cm^{-1}. The HD and D_2 species at 3630 cm^{-1} and 2989 cm^{-1} respectively are integrated from 3695 to 3550 cm^{-1} for HD and from 3050 to 2915 cm^{-1} for D_2. Finally, the methodology to calculate the conversion of D_2O and H_2 as well as the yield of HOD, HD and D_2 from the ATR-FTIR and Raman spectra is presented in details in the **ESI 2**.

Results and discussion

1. Description of infrared and Raman spectra

In a first set of experiments, the catalytic H/D exchange was studied in the presence of Ru/Al_2O_3. The **Fig. 3** displays ATR spectra of the liquid phase during this exchange. Initially, a spectrum is recorded before starting the kinetic experiments and vibrational bands of D_2O are observed with the two characteristic bands at 1205 cm^{-1} and 2480 cm^{-1} which correspond to the bending mode ν_2 (D-O-D) and the asymmetric stretching contribution ν_3 (O-D) of D_2O. After the insertion of H_2, a weak peak at around 1700 cm^{-1} is observed probably due to traces of acetone residue (after the cleaning of the cell) that disappear after 10 min of reaction.

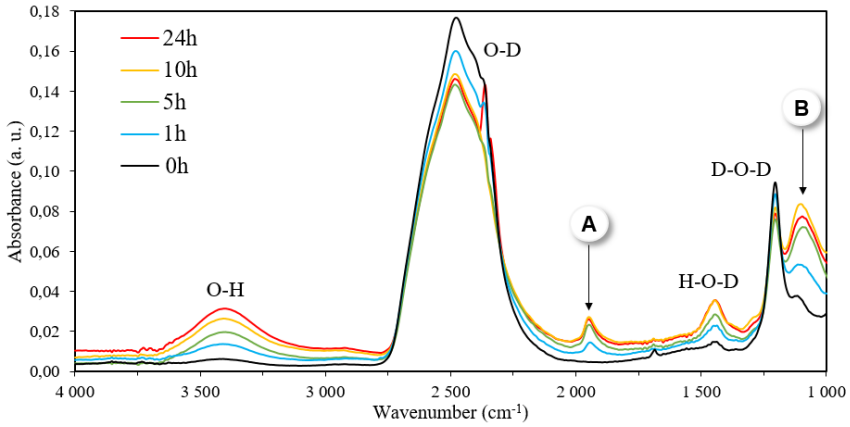

Figure 3: Spectra of the liquid phase obtained by ATR-FT-R spectroscopy during the catalytic H/D exchange between D_2O and H_2 in the presence of Ru/Al_2O_3 at 22 °C for 24 h under 30 bar of H_2.

ATR spectra are recorded during 24 h and show that two bands at 1456 cm^{-1} and 3401 cm^{-1} are increasing according to time. These bands are linked to the formation of HOD species and they correspond to the bending mode ν_2 (H-O-D) at 1456 cm^{-1} and the stretching contribution (O-H) at 3401 cm^{-1}. The stretching (O-D) of HOD is also visible around 2480 cm^{-1} but it coincides with the ν_3 (O-D) of D_2O explaining the shoulder observed around 2400 cm^{-1}. It is also noticed that two bands at 1947 cm^{-1} (A) and at 1100 cm^{-1} (B) are observed only in the case of Ru/Al_2O_3 catalyst and the identification of these bands will be discussed later.

Simultaneously to the analysis of the liquid phase by ATR, Raman scattering is used for the monitoring of the gas phase during the catalytic H/D exchange of H_2 and D_2O with Ru/Al_2O_3. Spectra are displayed in the **Fig. 4** in the low and high frequency range from 100 to 1100 cm^{-1} and from 2900 to 4250 cm^{-1}. Broad bands due to the fluorescence of the sapphire windows are present in these regions as it is shown in the black spectrum before the insertion of H_2 in the cell.

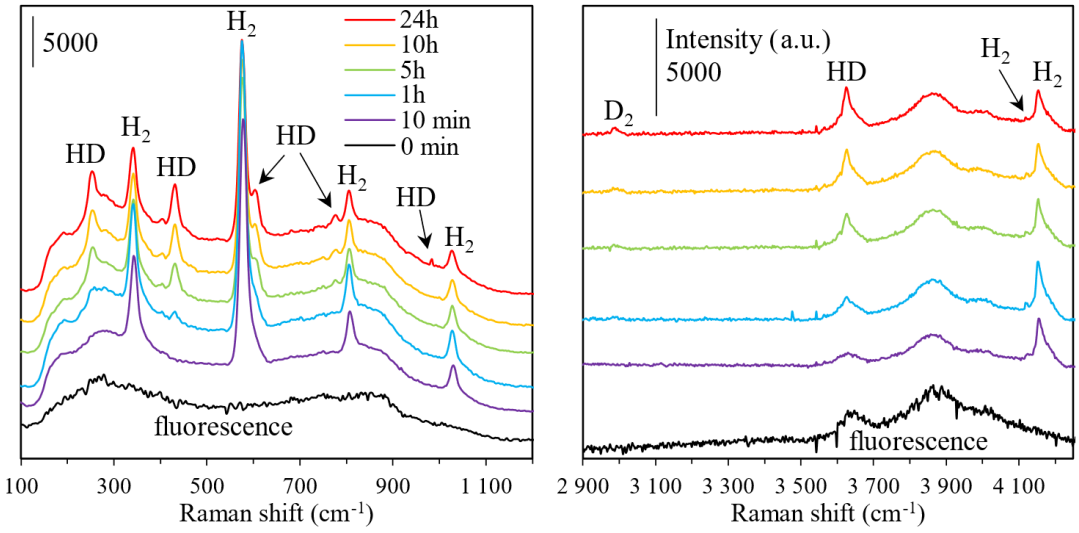

Figure 4: Spectra of the gas phase obtained by Raman spectroscopy during the catalytic H/D exchange between D_2O and H_2 in the presence of Ru/Al_2O_3 at 22 °C for 24 h under 30 bar of H_2.

When H_2 is added, rotational bands of H_2 are observed at 343, 580, 806 and 1031 cm^{-1} and are related to the S branch ($\Delta J=+2$) from 0 to 3rd rotational level respectively [29–31]. The

stretching vibration of H_2 (also called the vibrons) is Raman active with a main contribution at 4152 cm^{-1} that corresponds to Q_1 (J=1) and a weak peak at about 4125 cm^{-1} that corresponds to Q_1 (J=3) [29,30,32] is also observed but in less extent after 24 h. Because the pressure of H_2 takes time to equilibrate, the signal at 10 min is lowered compared to the signal at 1 h and, after this time, bands of H_2 are decreasing. Concomitantly to this decrease, peaks at 253, 434, 610, 774 and 980 cm^{-1} are increasing during the experiment of 24 h and they correspond to rotational contributions of HD with the S branch from 0 to 4^{th}. In the high frequency range, vibrons of HD at 3630 cm^{-1} (Q_1 (J=0)) is observed and it coincides with one band of fluorescence. More, a weak contribution at 2989 cm^{-1} appears and corresponds to the Q_1 (J=0) stretch vibrons of D_2 species.

Acquisitions of infrared and Raman spectra during the catalytic H/D exchange demonstrate that HOD, HD and D_2 species are simultaneously produced in liquid and gas phase in the presence of Ru/Al_2O_3 and the attribution of spectral bands are summarized in the **ESI 3**. To verify that the H/D exchange comes from the catalyst, same experiment is performed but without catalyst and no D_2O nor H_2 are consumed, as expected [26,27]. These first results already confirm that Ru catalyst is able to perform the H/D exchange.

2. Kinetic profiles of D_2O, H_2, HOD, HD and D_2 species

Raman scattering spectra and infrared spectra are recorded simultaneously which allow to correlate without ambiguity the kinetic profiles of D_2O and H_2 that are converted into HOD, HD and D_2 species.

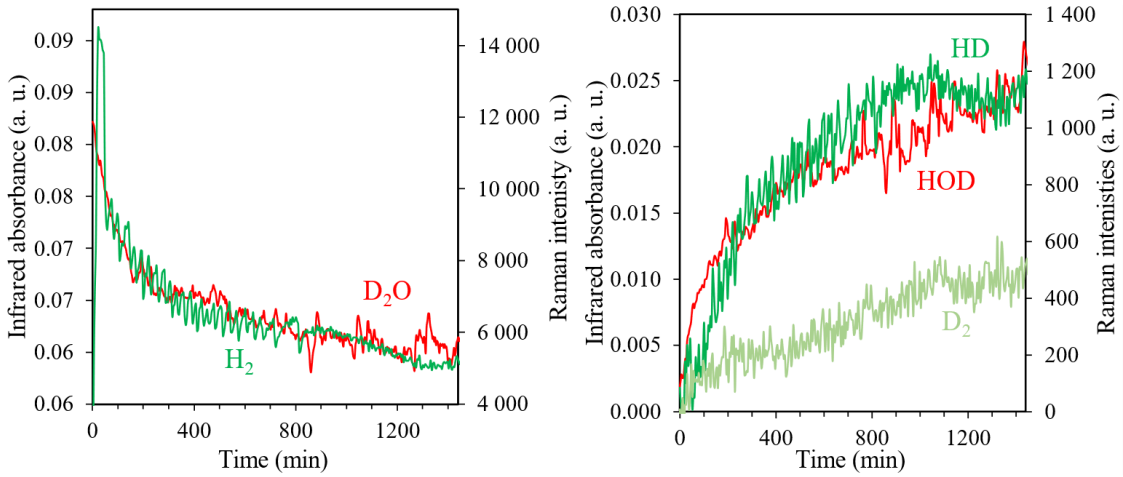

Figure 5: Kinetic profiles of D_2O (1205 cm^{-1}) and HOD (1450 cm^{-1}) obtained by ATR-FT-IR analysis (in red) as well as kinetic profiles of H_2 (579 cm^{-1}), HD (3625 cm^{-1}) and D_2 (2988 cm^{-1}) obtained by Raman measurements (in green) during the catalytic H/D exchange between D_2O and H_2 over Ru/Al_2O_3 at 22 °C for 24 h under 30 bar of H_2.

The **Fig. 5** displays kinetic profiles obtained by infrared (D_2O and HOD in red) and by Raman analysis (H_2, HD and D_2 in green) during the catalytic H/D exchange with Ru/Al_2O_3. Kinetics of D_2O and H_2 have similar profiles with a quick decrease at the first 200 min of the experiment following by a less marked decrease for the last 1440 min. The signal of H_2 shows however, a rapid increase to higher intensities and then a fast decrease during the first 100 min of the reaction that is considered as an "induction" time for H_2 to reach equilibrium between the liquid and the gas phase.

In accordance with the decrease of H_2 and D_2O signals, profiles of HOD, HD and D_2 are increasing according to time justifying that these species are produced from the catalytic exchange between H_2 and D_2O. The formation of HOD and HD displays similar kinetic profiles with a strong increase at the first 200 min following by a less pronounced increase. Concerning D_2, its formation is slower than HD and the intensity of the D_2 signal is about half that of the HD signal.

Kinetic profiles in **Fig. 5** demonstrate that D_2O and H_2 are both firstly converted into HOD and HD as described in **Eq. 1**. The HD previously produced can then react with D_2O to produce D_2 species like in **Eq. 2**. The **Eq. 3** is the overall reaction starting from D_2O and H_2 to HOD and D_2 without HD as intermediate as suggested by Kurita and Sajiki's group [26,27].

$$D_2O + H_2 \rightarrow HOD + HD \qquad \textbf{Eq. 1}$$

$$D_2O + HD \rightarrow HOD + D_2 \qquad \textbf{Eq. 2}$$

$$2D_2O + H_2 \rightarrow 2HOD + D_2 \qquad \textbf{Eq. 3}$$

Then, in order to compare the efficiency of Ru/Al_2O_3 with Pt/Al_2O_3 and Pd/Al_2O_3, we have reported in **Fig. 6** the kinetics profiles of D_2O and HOD during the H/D exchange between D_2O and H_2 for 24 h at ambient temperature for the three catalysts. As for Ru/Al_2O_3, the H/D exchange occurs when Pt or Pd are used because D_2O band decreases and HOD bands increase meaning that D_2O is converted to HOD.

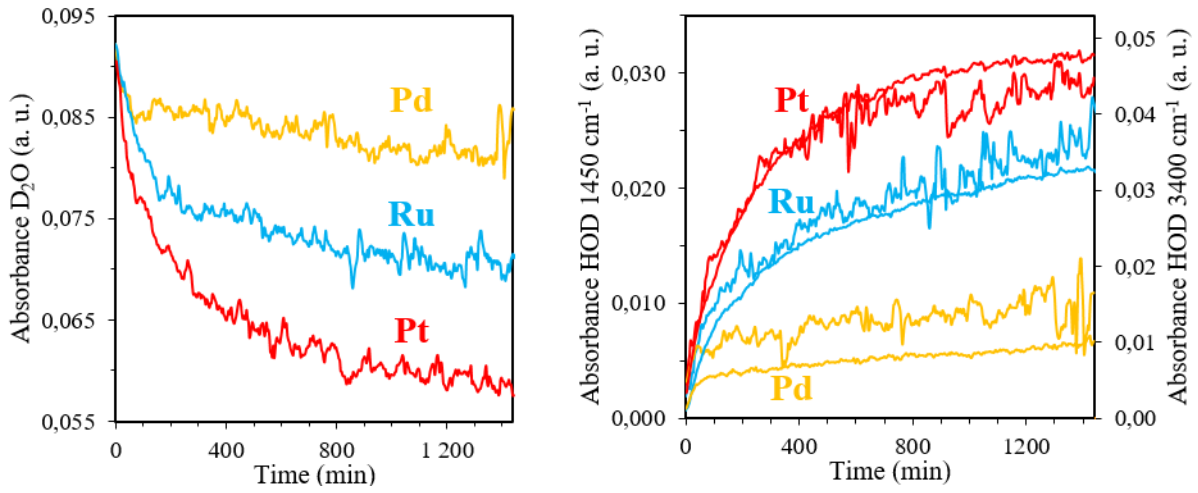

Figure 6: Kinetic profiles of D_2O at 1205 cm^{-1} and of HOD at 1450 cm^{-1} (noisy) and at 3400 cm^{-1} during the H/D exchange between D_2O and H_2 over Ru, Pt and Pd/Al_2O_3 at 22 °C for 24 h under 30 bar of H_2.

However, we observe qualitatively that activities of H/D exchange depend on the metal used. These kinetics demonstrate that for all catalysts tested, the conversion of D_2O to HOD is possible and the catalytic efficiency of the metal to perform the H/D exchange is as follows: $Pt/Al_2O_3 > Ru/Al_2O_3 >> Pd/Al_2O_3$.

From these kinetic profiles, the conversion and yields of the H/D exchange were determined after 24 h of reaction at ambient temperature. Thus, **Fig. 7** displays the number of mol of H_2 and D_2O that are consumed during the H/D exchange as well as the number of moles of produced HOD, HD and D_2 for the different catalysts used. For the number of moles of H_2

and of HOD, they were calculated using two different characteristic peaks of each species. Thus, we obtain an overall agreement between the two sets of data with an uncertainty of about +/- 10% that is due to all the sources of errors associated with our methodology (baseline correction, molar extinction coefficient, signal-to-noise ratio, spectrometer and laser stability). On the other hand, we emphasize that the number of initial moles of D_2O and H_2 differs (1.66 10^{-2} mol for D_2O and 5.95 10^{-3} mol for H_2) and therefore conversion of D_2O and H_2 cannot be directly compared. However, the conversion of D_2O with HOD yields and H_2 conversion with HD and D_2 yields can be quantitatively compared (conversions and yields are noted at the top of bars).

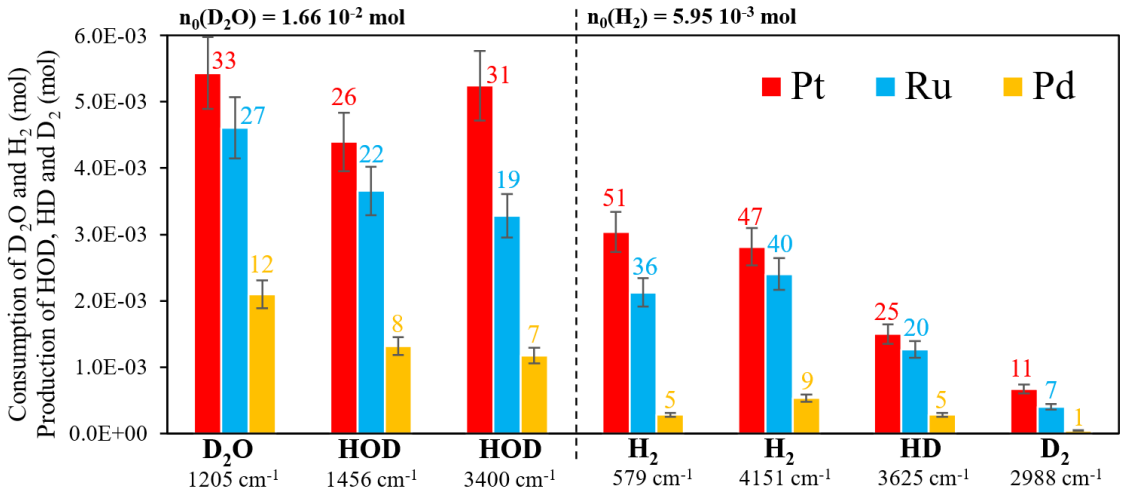

Figure 7: Number of mol consumed for D_2O (n_0 = 1.66 10^{-2} mol) and H_2 (n_0 = 5.95 10^{-3} mol) and number of mol produced of HOD, HD and D_2 after 24 h of H/D exchange at 22 °C with Pt, Ru or Pd/Al_2O_3 used as catalysts. On top of bars are indicated average conversions (for D_2O and H_2) and yields (for HOD, HD, D_2) in percentages.

In the case of the H/D exchange investigated with Pt/Al_2O_3 (red bars), the integration of the ν_2 infrared band of D_2O at 1205 cm^{-1} gives a conversion of around 33% with 5.4 10^{-3} mol of D_2O consumed. From the two contributions of HOD (ν_2 at 1456 cm^{-1} and ν_3 at 3400 cm^{-1}), we calculated a yield for HOD production of 26% (4.4 10^{-3} mol) and 31% (5.2 10^{-3} mol), respectively, that is in the error bars discussed above. Thus, the conversion of D_2O of 33% is roughly the same as the yield of HOD of 26-31% and demonstrate that D_2O is selectively converted into HOD.

In the same way, integration of Raman contribution S_1 at 579 cm^{-1} and Q_1 at 4151 cm^{-1} are used for H_2 measurements while stretch vibrons at 3625 cm^{-1} and at 2988 cm^{-1} are used to calculate the amount of HD and D_2 respectively. During the H/D exchange with Pt/Al_2O_3, the H_2 conversion is of 47-51% with 2.8-3.0 10^{-3} mol consumed. This is higher than the production of total products HD + D_2 given 36% of yields together and that corresponds to the formation of 2.2 10^{-3} mol. Although we expect to have same values for the conversion and the total yields, the reported difference of more than 10% is probably due to analytical approximation considered in our methodology to determine the concentration of HD and D_2.

However, it is clear that more HD is produced than D_2. An HD yield of 25% (1.5 10^{-3} mol) is obtained compared to 11% (6.7 10^{-4} mol) for D_2, suggesting that some HD intermediate

remained unreacted according to the **Eq. 2**. The number of moles comparison between D_2O (5.4 10^{-3} mol) and H_2 (2.8-3.0 10^{-3} mol) as well as HOD (4.4-5.2 10^{-3} mol) and HD + D_2 (2.2 10^{-3} mol) agree with the **Eq. 3** where twice more D_2O and HOD are needed to perform the reaction to lead to D_2 species.

When Ru/Al_2O_3 and Pd/Al_2O_3 are used for the H/D exchange of H_2 with D_2O, same interpretations as Pt/Al_2O_3 can be made except that conversion and yields are lower. In the case of Ru/Al_2O_3, 4.6 10^{-3} mol of D_2O gives 3.3-3.7 10^{-3} mol of HOD and twice less of H_2 with 2.1-2.4 10^{-3} mol that is transformed into 1.3 10^{-3} mol of HD and 6.7 10^{-4} mol of D_2. For Pd/Al_2O_3 the lowest conversions of D_2O and H_2 are recorded with 2.1 10^{-3} mol and 2.8-5.3 10^{-4} mol respectively giving 1.2-1.3 10^{-3} mol of HOD, 2.8 10^{-4} mol of HD and traces of D_2 with 4.2 10^{-5} mol.

Altogether, kinetic and quantification studies demonstrate that the H/D exchange between D_2O and H_2 is effective whatever the catalyst used but performance is dependent on the metal used. Catalyst Pt/Al_2O_3 shows the best performance, followed closely by Ru/Al_2O_3 while Pd/Al_2O_3 has the worst performance. These results do not explain why Ru/Al_2O_3 was the most efficient catalyst in the hydrogenation of glucose to sorbitol (**Table 1**). Finally, the effect of pressure and temperature on the catalytic isotopic H/D exchange with Ru/Al_2O_3 has been investigated and the conversion of D_2O and H_2 as well as the yield of HOD, HD and D_2 after 24 h of reaction are reported in the **ESI 4**. In particular, the increase of temperature enhances the conversion and yield of the reaction.

As proposed in recent articles, the catalytic isotopic H/D exchange between D_2O and H_2 could process through proton-shuttle and proton-electron transfer mechanism [14,19]. The gas H_2 dissociates homolytically and two H* adsorb on the metal surface. Nearby water molecules interact with H* and form ionized H_2O-H^+ accompanied by an electron that transfers to the metal's *d*-band. Proton of H_2O-H^+ is located at the solid-liquid interface and can easily delocalize through water molecules by proton-shuttling to reach the carbonyl function when the substrate is added in the media. Following this mechanism, the H/D exchange with D_2O and H_2 involves a D_2O^+-H intermediate that can be schematized as in the **Fig. 8**.

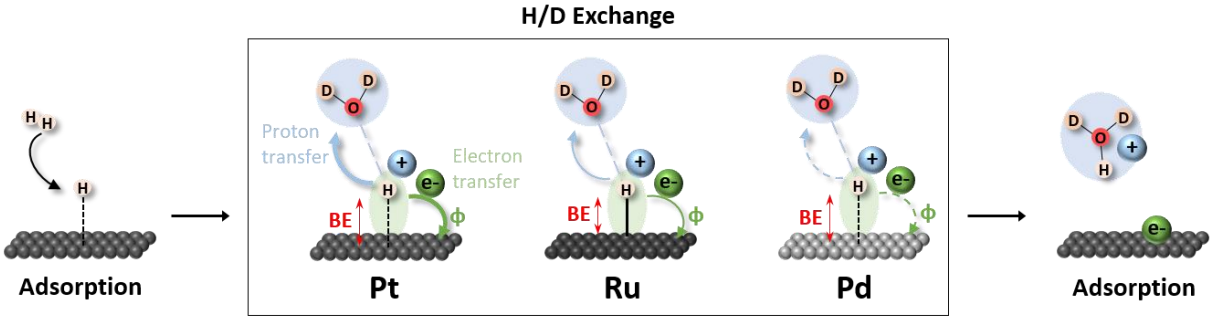

Figure 8: Formation of the intermediate D_2O-H^+ during the isotopic H/D exchange of D_2O and H_2 on metal surfaces inspired by reference [33].

As explained by Hensley *et al.*[34], the ability of the metal to convert an adsorbed H* into H^+ is two-fold. It implies to break the bond between H* and the metal but also to transfer an electron into the metal's *d*-band. These two characteristics were calculated by DFT for

Pt(111), Ru(0001) and Pd(111) [35] where the binding energy (BE) defines the strength of the M-H* bond while the work function (φ) is related to the minimum energy required to move electrons into the metal surface. BE and φ for each metal are reported in the **Table 2**. We emphasize that (0001) surface rather than (111) surface of Ru is chosen as Ru(0001) has become a benchmark system for investigation of Ru catalysed hydrogenation reactions in water [19,36,37].

Table 2: Binding energies (BE) and work function (φ) on hydrogen adsorption for Pt(111), Ru(0001) and Pd(111) calculated at the vapor interface by Ferrin et al. [35].

	BE (eV)	**φ (eV)**
Pt	-2.72	-0.06
Ru	-2.97	0.03
Pd	-2.88	0.08

The BE of Pt(111) is the lowest one with -2.72 eV and its φ is the lowest one with -0.06 eV. In comparison to Ru(0001) and Pd(111), these results means that for Pt(111) the bond Pt-H* can disrupt more easily and its ability to transfer electrons is also higher, both properties that would favor the H/D exchange. The BE of Pd(111) is lower by 0.09 eV compared to Ru(0001) whereas the φ of Ru(0001) is lower by 0.05 eV to Pd(111). Therefore, although the disrupt of the Pd-H* bond is easier than for Ru, the lower energy needed to transfer electrons in Ru *d*-band compared to Pd *d*-band seems to be the main factor that drives the H/D exchange explaining the higher activity of Ru/Al_2O_3 in comparison with Pd/Al_2O_3.

Therefore, from the BE and φ values reported in **Table 2**, we can qualitatively explain why the catalytic efficiency of the metal to perform the H/D exchange is in the order: $Pt/Al_2O_3 > Ru/Al_2O_3 >> Pd/Al_2O_3$.

Clearly, the mechanism involved in the hydrogenation of glucose cannot be fully interpreted from the kinetics investigation on the model reaction of H/D exchange between D_2O and H_2. However, when using Ru/Al_2O_3 as the catalyst, we have observed on the ATR-FTIR spectra of the water phase for both the catalytic H/D exchange or glucose hydrogenation an absorption band at about 1950 cm^{-1} that we defined as the Ru-band (see **Fig. 9** and **Fig. S4** in **ESI 5**). The next part is dedicated to the attribution of this band to a transient species that could explain the higher efficiency of Ru/Al_2O_3 for the hydrogenation of glucose.

3. Assignment of the Ru-band to Ru-H species

The **Fig. 9** displays the spectra of the Ru-band (A) (1947 cm^{-1}), of the Ru-band (B) (1100 cm^{-1}) and of HOD (1450 cm^{-1}) as well as their kinetic profiles obtained during the H/D exchange over Ru/Al_2O_3. The identity of the Ru-Band (A) and (B) band is unknown but it is supposed to be related to the metal Ru because they do not appear when Pt and Pd are used as catalysts for the H/D exchange. Moreover, the increase of the Ru-band (A) and (B) is not directly linked to the formation of HOD species obtained during the catalytic H/D exchange as their kinetic profiles differs. However, the kinetic of the Ru-band (A) and (B) are very similar showing that they might be related to the same species.

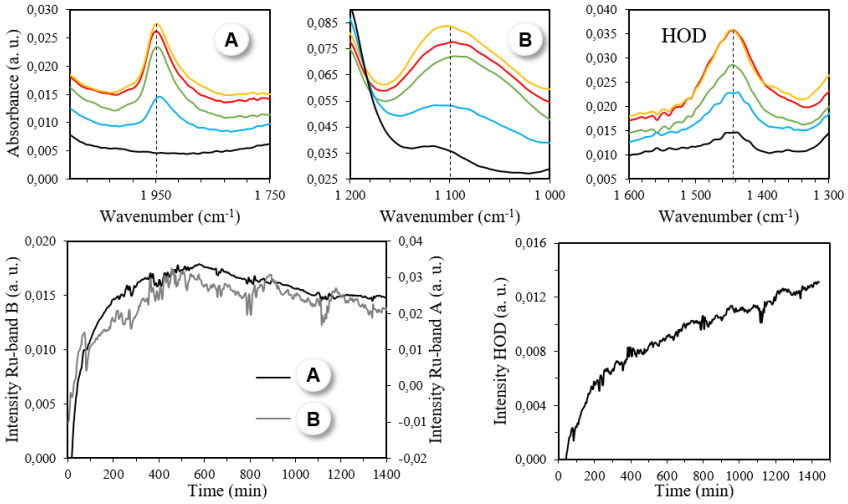

Figure 9: Spectra and kinetic profiles of HOD (1450 cm^{-1}), the Ru-band (A) at 1947 cm^{-1} and Ru-band (B) at 1100 cm^{-1} obtained by ATR-FT-IR during the H/D exchange between D_2O and H_2 in the presence of Ru/Al_2O_3 at 22 °C.

Interestingly, the Ru-band (A) is also observed during the hydrogenation of glucose to sorbitol (see ATR-FTIR spectra in **ESI 5- Fig. S4**) suggesting that the same species is involved during both the H/D exchange and the hydrogenation reaction. However, the contribution of the Ru-band (B) is more difficult to analyze in the presence of glucose as some contributions in this frequency range are also related to glucose. In addition, this spectral range is also characteristic of Al_2O_3 that has a strong absorption around 1100 cm^{-1} that could eventually lead to fluctuations of the intensity of the ATR-IR signal in this region. Therefore, we will focus the discussion below on the Ru-band (A) that was clearly put in evidence in all the catalytic experiments performed in water using Ru/Al_2O_3.

A possible attribution of this Ru-band (A) band could be to the formation of carbonyl species at the surface of Ru. Indeed, Ferri *et al.* have determined by ATR-FTIR studies that the addition of solvent dichloromethane can clean the metal surface at ambient temperature and that the addition of H_2 in solvent allowed to desorb contaminants on the surface of Pt by the assignment of carbonyl species [38]. Such behavior can be transpose to our experiment where solvent water and dissolved H_2 enhance desorption of carbonyl to give the characteristic Ru-band.The adsorption of carbonyl in linear or bridge configuration on metal surface was largely studied in the literature especially on Pt and Pd as well as Ru but to a lesser extent [39–47]. Baiker's group especially assigned carbonyl adsorbed linearly on Ru/Al_2O_3 at 2006 cm^{-1} by ATR-FTIR after the insertion of 5 bar of CO at 50 °C and interestingly the appearance of the Ru-CO(L) band is like our study with a characteristic broad shape [42].

In order to clarify the possible role of CO in the observation of the Ru-peak, gaseous CO is directly added on "deposited" Ru/Al_2O_3 in pure gas conditions or in aqueous environment. Ru/Al_2O_3 was deposited on the silicon crystal for ATR-FTIR measurements and on a metallic screw for IR microscopy measurements in reflection mode (see **ESI 6-Fig. S5**). The spectra are displayed in **ESI 7-Fig. S6**. The formation of carbonyl group adsorbed on the surface of Ru/Al_2O_3 in a water environment leads to two vibrational bands at 2060 cm^{-1} and 2010 cm^{-1} that could be assigned to linear and bridge carbonyls. As two bands are observed and

that the shape of the band does not correspond to the Ru-band observed at 1947 cm^{-1} during the H/D exchange and the glucose hydrogenation, it confirms that the Ru-band cannot be carbonyl species.

Another possible assignment of the Ru-band (A) could be the stretching mode of Ru-H intermediate that are formed when H_2 gas dissolves in D_2O and then adsorbs on the surface of the metal before the exchange reaction. As it was previously mentioned in the **Table 2**, the BE of Ru(0001) is the highest one compared to Pt(111) and Pd(111). It means that the Ru-H specie might be more stable than the Pt-H or Pd-H intermediate explaining the presence of the band at 1947 cm^{-1} only in the case of Ru/Al_2O_3.Therefore, the apparition of the Ru-band for both the H/D exchange and the hydrogenation can be an indication to explain why Ru/Al_2O_3 is active for the hydrogenation of glucose while Pt/Al_2O_3 and Pd/Al_2O_3 are inactive.

To demonstrate that the Ru-band at around 1950 cm^{-1} is actually a Ru-H intermediate, the Ru/Al_2O_3 is firstly studied by ATR-FTIR through the deposition of a thin film of the solid at the surface of the silicon crystal to probe intermediate species [48]. But after 24 h under pressure of 30 bar of H_2, the Ru-band is not observed. A deposit of Ru/Al_2O_3 under pressure of H_2 is also studied by infrared reflection (see **ESI 6-Fig. S5** for the description of the cell) where the sensitivity to detect adsorbed species should be enhanced (higher thickness of Ru/Al_2O_3 deposit) but no band at around 1950 cm^{-1} is observed. Consequently, when only pressure of gaseous H_2 is in contact with Ru/Al_2O_3, no change is observed in infrared spectra whereas the Ru-band constantly appears in aqueous environment. On the other hand, the replacement of D_2O by H_2O does not result to a significant shift of the Ru-band when H_2 pressure is added (see ATR-FTIR spectra in **ESI 8-Fig. S7**). Then, water plays a crucial role to observe the Ru-band but does not seem directly involved in the vibrating species. Therefore, the Ru-band could be an intermediate Ru-H as previously mentioned, however, on the contrary of adsorbed carbonyls, only few studies have been focused on infrared studies of the formation of Ru-H surface species in the gas phase and, to our knowledge none in the aqueous phase. Ishikawa *et al.* have studied the adsorption of H_2 on Ru/ZrO_2 by FTIR spectroscopy, they assume that the peak of Ru-H species should appear between 1800 and 2000 cm^{-1}, which is in accordance with our experimental data, but they do not have observed Ru-H species experimentally [49]. Others have performed studies of H_2 adsorption on Ru/Al_2O_3 and no band of H_2 adsorbed on bare Ru surface appeared. However, when CO is pre-adsorbed, they assume the formation of a hydrocarbonyl species H-Ru-CO at around 2030 cm^{-1} [41] which could be possibly formed in our study.

Recent articles have explored various adsorption states of H_2 on Ru nanoparticles by infrared spectroscopy and performed DFT calculations using a nanoscale Ru particle model (Ru_{153}) to assign the vibrational frequencies of the infrared spectra observed for Ru/MgO exposed to H_2 gas [50,51]. It turns out that in the experiment involving switching between H_2 and Ar at 250 °C, the introduction of H_2 on Ru/MgO surface increased infrared absorbance and induced the appearance of two peaks at 1998 cm^{-1} and at 1863 cm^{-1}. DFT calculations assigned the former peak to H_2 horizontally adsorbed on top of a bridge Ru atom. In contrast, the peak at 1863 cm^{-1} did not correspond to the adsorption of H_2 on the Ru surface, as this activated H_2 observed at 1998 cm^{-1} is found to have a short lifetime, but rather corresponds to the binding of

a hydrogen atom on Ru_{153}. Indeed, DFT calculations show that an H atom binding "on top site" of Ru_{153} (Ru-H) leads to a Ru-H stretching band at 1852 cm^{-1} in good agreement with the experimental peak at 1863 cm^{-1}. Therefore, these experimental and calculated frequencies of Ru-H species on MgO surfaces are in the same spectral range than the Ru-band (A) observed for our Ru/Al_2O_3 surface in water located between 1940 cm^{-1} and 1970 cm^{-1} hence supporting our hypothesis that the Ru band (A) can be assigned to a Ru-H stretching band that results from an activated form of H* binding "on top site" on the Ru/Al_2O_3 surface. In addition, these DFT calculation reports other possible Ru-H stretching bands at about 1000 cm^{-1} associated with H atoms in "bridge" configurations with 4 Ru atoms that might be associated with the experimental Ru-Band (B) peak at 1100 cm^{-1} (see fig. S9 of reference [51]).

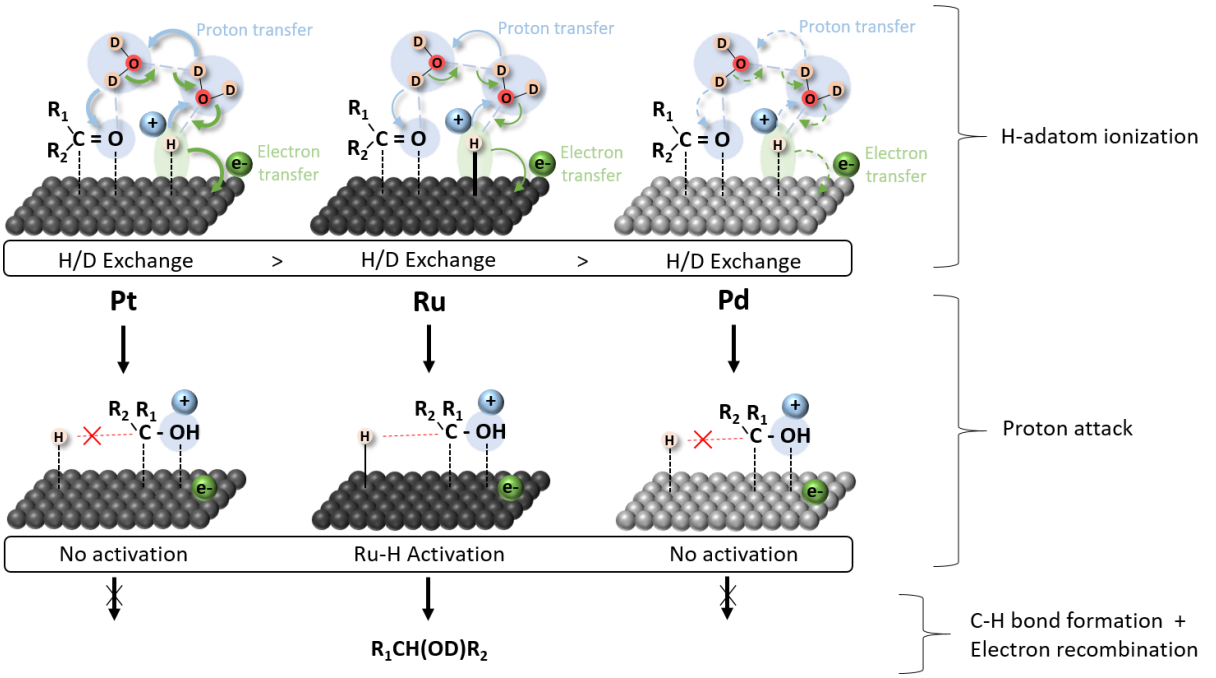

Figure 10: Proposed sequence of elementary steps for the hydrogenation of carbonyl over Pt, Ru and Pd metal surfaces.

Thus, the observation of the Ru-H band by ATR-FTIR could explain that these H atoms "on top" and "bridge" configurations are only detected on the surface of Ru but not for other metals. Such configuration observed only for Ru could be explained by the fact that the valence electronic structure of Ru (4d7 5s1) differs from that of Pt (5d9 6s1) and Pd (4d10). Indeed, a H binding to a unique Pd atom is very unlikely as its valence shell is full. Also, even if a H binding to a unique Pt atom is possible [52], it is much less probable than for Ru. On the other hand, H atoms that can interact with 2, 3 or 4 atoms in "bridge" configurations might exist for Pd-Pt metal surface but seems to be favored for Ru [51]. Thus, the observation of the Ru-band could explain that adsorbed H* are more activated on the surface of Ru than on other metals. In particular, the presence of H atom binding "on top site" of Ru that are more sterically accessible and less bounded to the surface than in bridge configurations (see reference [51]) could explain the easier H transfer to the carbon atom of the carbonyl for the hydrogenation of glucose to sorbitol. Indeed, in the glucose hydrogenation mechanism, we might infer that the kinetically relevant step concerns the addition of one adsorbed H* on the carbon atom of the carbonyl [19] and the "better" activation of adsorbed H* on Ru could enhance this step (see

Fig. 10). We emphasize that the prevalence of proton-electron transfer during the catalytic hydrogenation of the first H atom to the oxygen of the carbonyl in water on Ru surfaces is supported experimentally by kinetic measurements with H-D isotopic studies.[19] In particular they used D_2 instead of H_2 in few experiments under a pressure of 1.3 bar. Such kind of experiments could have been performed in this work but this was beyond the scope of our study.

Conclusion

This work emphasizes a possible reason why the metal Ru is efficient for the hydrogenation of glucose, and to a larger extent, the hydrogenation of various aldoses and carboxylic derivatives in aqueous media. Indeed, we have demonstrated in a previous work that Ru/Al_2O_3 is very effective to convert glucose into sorbitol whereas the noble metal Pt and Pd are inactive. Herein, it was demonstrated here that the proton transfer of H ad-atoms to water plays a key role in the hydrogenation mechanism. This mechanism is followed by the catalytic H/D exchange between H_2 and D_2O to give HOD, HD and D_2 that are measured *in operando* with the simultaneous coupling of ATR-IR and Raman spectroscopy. After 24 h at 22 °C under 30 bar of H_2, the efficiency of catalysts for the H/D exchange is Pt/Al_2O_3 > Ru/Al_2O_3 >> Pd/Al_2O_3 showing that the H/D exchange between D_2O and H_2 is effective whatever the catalyst used but performance is dependent on the nature of the metal. Distinctively, an infrared band located around 1950 cm^{-1} observed only with Ru/Al_2O_3, is tentatively assigned to H atoms adsorbed and activated on the Ru surface. This H* could be directly added to the carbon atom of the carbonyl of glucose to give sorbitol in a more efficient way compared to the other metals where this band is not observed. Thus, this peculiarity observed only in the case of Ru/Al_2O_3 could explain its enhanced activity in the hydrogenation of glucose in aqueous media, and to a larger extent, its high efficiency for the hydrogenation of various aldoses and carboxylic derivatives in water.

ACKNOWLEDGMENTS

The authors acknowledge the Region Nouvelle Aquitaine and the University of Poitiers for their financial support for the funding of the PhD of I. Bonnin. They are also grateful to the program "Défi in situ en conditions extrêmes" of the MITI of CNRS for the financial support to the infrared and Raman equipment, to INCREASE Federation and to the GDR 2035 SolvATE.

References

[1] J.J. Bozell, G.R. Petersen, Technology development for the production of biobased products from biorefinery carbohydrates—the US Department of Energy's "Top 10" revisited, Green Chem. 12 (2010) 539–554. https://doi.org/10.1039/B922014C.

[2] P. Gallezot, P.J. Cerino, B. Blanc, G. Flèche, P. Fuertes, Glucose hydrogenation on promoted raney-nickel catalysts, Journal of Catalysis. 146 (1994) 93–102. https://doi.org/10.1016/0021-9517(94)90012-4.

[3] N. Déchamp, A. Gamez, A. Perrard, P. Gallezot, Kinetics of glucose hydrogenation in a trickle-bed reactor, Catalysis Today. 24 (1995) 29–34. https://doi.org/10.1016/0920-5861(95)00019-C.

[4] H. Li, W. Wang, J. Fa Deng, Glucose Hydrogenation to Sorbitol over a Skeletal Ni-P Amorphous Alloy Catalyst (Raney Ni-P), Journal of Catalysis. 191 (2000) 257–260. https://doi.org/10.1006/jcat.1999.2792.
[5] H. Li, H. Li, J.-F. Deng, Glucose hydrogenation over Ni–B/SiO2 amorphous alloy catalyst and the promoting effect of metal dopants, Catalysis Today. 74 (2002) 53–63. https://doi.org/10.1016/S0920-5861(01)00530-2.
[6] J.-P. Wen, C.-L. Wang, Y.-X. Liu, Preparation of sorbitol from D-glucose hydrogenation in gas–liquid–solid three-phase flow airlift loop reactor, Journal of Chemical Technology & Biotechnology. 79 (2004) 403–406. https://doi.org/10.1002/jctb.1001.
[7] S. Schimpf, C. Louis, P. Claus, Ni/SiO2 catalysts prepared with ethylenediamine nickel precursors: Influence of the pretreatment on the catalytic properties in glucose hydrogenation, Applied Catalysis A: General. 318 (2007) 45–53. https://doi.org/10.1016/j.apcata.2006.10.034.
[8] R. Geyer, P. Kraak, A. Pachulski, R. Schödel, New Catalysts for the Hydrogenation of Glucose to Sorbitol, Chemie Ingenieur Technik. 84 (2012) 513–516. https://doi.org/10.1002/cite.201100108.
[9] A. Corma, S. Iborra, A. Velty, Chemical Routes for the Transformation of Biomass into Chemicals, Chem. Rev. 107 (2007) 2411–2502. https://doi.org/10.1021/cr050989d.
[10] M. Besson, P. Gallezot, C. Pinel, Conversion of Biomass into Chemicals over Metal Catalysts, Chem. Rev. 114 (2014) 1827–1870. https://doi.org/10.1021/cr4002269.
[11] I. Bonnin, R. Méreau, T. Tassaing, F. Jérôme, K. De Oliveira Vigier, Hydrogenation of Sugars to Sugar Alcohols in the Presence of a Recyclable Ru/Al2O3 Catalyst Commercially Available, ACS Sustainable Chem. Eng. (2021). https://doi.org/10.1021/acssuschemeng.1c01422.
[12] C. Michel, J. Zaffran, A.M. Ruppert, J. Matras-Michalska, M. Jędrzejczyk, J. Grams, P. Sautet, Role of water in metal catalyst performance for ketone hydrogenation: a joint experimental and theoretical study on levulinic acid conversion into gamma-valerolactone, Chem. Commun. 50 (2014) 12450–12453. https://doi.org/10.1039/C4CC04401K.
[13] C. Michel, P. Gallezot, Why Is Ruthenium an Efficient Catalyst for the Aqueous-Phase Hydrogenation of Biosourced Carbonyl Compounds?, ACS Catal. 5 (2015) 4130–4132. https://doi.org/10.1021/acscatal.5b00707.
[14] Z. Zhao, R. Bababrik, W. Xue, Y. Li, N.M. Briggs, D.-T. Nguyen, U. Nguyen, S.P. Crossley, S. Wang, B. Wang, D.E. Resasco, Solvent-mediated charge separation drives alternative hydrogenation path of furanics in liquid water, Nat Catal. 2 (2019) 431–436. https://doi.org/10.1038/s41929-019-0257-z.
[15] B. Demir, T. Kropp, E.B. Gilcher, M. Mavrikakis, J.A. Dumesic, Effects of water on the kinetics of acetone hydrogenation over Pt and Ru catalysts, Journal of Catalysis. (2021). https://doi.org/10.1016/j.jcat.2021.03.013.
[16] Z. Wu, Y.-H.C. Chin, Catalytic pathways and mechanistic consequences of water during vapor phase hydrogenation of butanal on Ru/SiO2, Journal of Catalysis. 394 (2021) 429–443. https://doi.org/10.1016/j.jcat.2020.10.022.
[17] Y. Dai, X. Gao, X. Chu, C. Jiang, Y. Yao, Z. Guo, C. Zhou, C. Wang, H. Wang, Y. Yang, On the role of water in selective hydrogenation of cinnamaldehyde to cinnamyl alcohol on PtFe catalysts, Journal of Catalysis. 364 (2018) 192–203. https://doi.org/10.1016/j.jcat.2018.05.008.
[18] A.J.R. Hensley, Y. Wang, D. Mei, J.-S. McEwen, Mechanistic Effects of Water on the Fe-Catalyzed Hydrodeoxygenation of Phenol. The Role of Brønsted Acid Sites, ACS Catal. 8 (2018) 2200–2208. https://doi.org/10.1021/acscatal.7b02576.
[19] J. Shangguan, Y.-H.C. Chin, Kinetic Significance of Proton–Electron Transfer during Condensed Phase Reduction of Carbonyls on Transition Metal Clusters, ACS Catal. 9 (2019) 1763–1778. https://doi.org/10.1021/acscatal.8b03470.
[20] J. Shangguan, A.J.R. Hensley, M.V. Gradiski, N. Pfriem, J.-S. McEwen, R.H. Morris, Y.-H.C. Chin, The Role of Protons and Hydrides in the Catalytic Hydrogenolysis of Guaiacol at the Ruthenium Nanoparticle–Water Interface, ACS Catal. 10 (2020) 12310–12332. https://doi.org/10.1021/acscatal.0c01963.

[21] W. Song, Y. He, S. Lai, W. Lai, X. Yi, W. Yang, X. Jiang, Selective hydrodeoxygenation of lignin phenols to alcohols in the aqueous phase over a hierarchical Nb2O5-supported Ni catalyst, Green Chem. 22 (2020) 1662–1670. https://doi.org/10.1039/C9GC03842F.
[22] Y. Kim, E. Moon, S. Shin, H. Kang, Acidic Water Monolayer on Ruthenium(0001), Angewandte Chemie. 124 (2012) 12978–12981. https://doi.org/10.1002/ange.201205756.
[23] L.R. Merte, G. Peng, R. Bechstein, F. Rieboldt, C.A. Farberow, L.C. Grabow, W. Kudernatsch, S. Wendt, E. Lægsgaard, M. Mavrikakis, F. Besenbacher, Water-Mediated Proton Hopping on an Iron Oxide Surface, Science. 336 (2012) 889–893. https://doi.org/10.1126/science.1219468.
[24] E. Yuan, Q. Li, P. Ni, P. Jian, Q. Deng, Microbehavior mechanism of water mediator on palladium in catalytic hydrogenation of aromatic carbonyl: Enhancement of hydrogen shuttling and modification of electronic structure, Molecular Catalysis. 514 (2021) 111872. https://doi.org/10.1016/j.mcat.2021.111872.
[25] K. Rahkamaa-Tolonen, T. Salmi, D.Yu. Murzin, L.B. Dillon, H. Karhu, R.L. Keiski, J. Väyrynen, Investigation of NO Reduction by H2 on Pd Monolith with Transient and Isotopic Exchange Techniques: I. H2/D2 Exchange with H2O and NH3, Journal of Catalysis. 210 (2002) 17–29. https://doi.org/10.1006/jcat.2002.3668.
[26] H. Sajiki, T. Kurita, H. Esaki, F. Aoki, T. Maegawa, K. Hirota, Complete replacement of H2 by D2 via Pd/C-catalyzed H/D exchange reaction, Org Lett. 6 (2004) 3521–3523. https://doi.org/10.1021/ol048591b.
[27] T. Kurita, F. Aoki, T. Mizumoto, T. Maejima, H. Esaki, T. Maegawa, Y. Monguchi, H. Sajiki, Facile and convenient method of deuterium gas generation using a Pd/C-catalyzed H2-D2 exchange reaction and its application to synthesis of deuterium-labeled compounds, Chemistry. 14 (2008) 3371–3379. https://doi.org/10.1002/chem.200701245.
[28] N.O. of D. and Informatics, Bienvenue sur le WebBook de Chimie NIST, (n.d.). https://doi.org/10.18434/T4D303.
[29] D.K. Veirs, G.M. Rosenblatt, Raman line positions in molecular hydrogen: H2, HD, HT, D2, DT, and T2, Journal of Molecular Spectroscopy. 121 (1987) 401–419. https://doi.org/10.1016/0022-2852(87)90058-0.
[30] L. Li, X. Zhang, Z. Luan, Z. Du, S. Xi, B. Wang, L. Cao, C. Lian, J. Yan, Raman vibrational spectral characteristics and quantitative analysis of H_2 up to 400°C and 40 MPa, J Raman Spectrosc. 49 (2018) 1722–1731. https://doi.org/10.1002/jrs.5420.
[31] D.V. Petrov, I.I. Matrosov, D.O. Sedinkin, A.R. Zaripov, Raman Spectra of Nitrogen, Carbon Dioxide, and Hydrogen in a Methane Environment, Opt. Spectrosc. 124 (2018) 8–12. https://doi.org/10.1134/S0030400X18010137.
[32] R.T. Howie, I.B. Magdău, A.F. Goncharov, G.J. Ackland, E. Gregoryanz, Phonon Localization by Mass Disorder in Dense Hydrogen-Deuterium Binary Alloy, Phys. Rev. Lett. 113 (2014) 175501. https://doi.org/10.1103/PhysRevLett.113.175501.
[33] T.R. Lee, G.M. Whitesides, Isotopic exchange in the platinum-catalyzed reductions of olefins in protic solvents, J. Am. Chem. Soc. 113 (1991) 2568–2576. https://doi.org/10.1021/ja00007a035.
[34] A.J.R. Hensley, J. Bray, J. Shangguan, Y.-H. (Cathy) Chin, J.-S. McEwen, Catalytic consequences of hydrogen addition events and solvent-adsorbate interactions during guaiacol-H2 reactions at the H2O-Ru(0 0 0 1) interface, Journal of Catalysis. 395 (2021) 467–482. https://doi.org/10.1016/j.jcat.2020.09.034.
[35] P. Ferrin, S. Kandoi, A.U. Nilekar, M. Mavrikakis, Hydrogen adsorption, absorption and diffusion on and in transition metal surfaces: A DFT study, Surface Science. 606 (2012) 679–689. https://doi.org/10.1016/j.susc.2011.12.017.
[36] A. Michaelides, A. Alavi, D.A. King, Different Surface Chemistries of Water on Ru{0001}: From Monomer Adsorption to Partially Dissociated Bilayers, J. Am. Chem. Soc. 125 (2003) 2746–2755. https://doi.org/10.1021/ja028855u.
[37] M.A. Ramzan, R. Wischert, S.N. Steinmann, C. Michel, Toward a Realistic Surface State of Ru in Aqueous and Gaseous Environments, J. Phys. Chem. Lett. (2023) 4241–4246. https://doi.org/10.1021/acs.jpclett.3c00313.

[38] D. Ferri, T. Bürgi, A. Baiker, Pt and Pt/Al $_2$ O $_3$ Thin Films for Investigation of Catalytic Solid−Liquid Interfaces by ATR-IR Spectroscopy: CO Adsorption, H $_2$ -Induced Reconstruction and Surface-Enhanced Absorption, J. Phys. Chem. B. 105 (2001) 3187–3195. https://doi.org/10.1021/jp002268i.
[39] T. Mizushima, K. Tohji, Y. Udagawa, A. Ueno, An EXAFS and IR study of the CO adsorption-induced morphology change in ruthenium catalysts, J. Am. Chem. Soc. 112 (1990) 7887–7893. https://doi.org/10.1021/ja00178a006.
[40] M. Marwood, R. Doepper, A. Renken, In-situ surface and gas phase analysis for kinetic studies under transient conditions The catalytic hydrogenation of CO2, Applied Catalysis A: General. 151 (1997) 223–246. https://doi.org/10.1016/S0926-860X(96)00267-0.
[41] S.Zh. Todorova, G.B. Kadinov, Infrared spectroscopy study of adsorption and coadsorption of carbon monoxide and hydrogen on Ru/Al203, Research on Chemical Intermediates. 28 (2002) 291–301. https://doi.org/10.1163/15685670260188601.
[42] M. Burgener, D. Ferri, J.-D. Grunwaldt, T. Mallat, A. Baiker, Supercritical Carbon Dioxide: An Inert Solvent for Catalytic Hydrogenation?, J. Phys. Chem. B. 109 (2005) 16794–16800. https://doi.org/10.1021/jp0521353.
[43] S.Y. Chin, C.T. Williams, M.D. Amiridis, FTIR Studies of CO Adsorption on Al2O3- and SiO2-Supported Ru Catalysts, J. Phys. Chem. B. 110 (2006) 871–882. https://doi.org/10.1021/jp053908q.
[44] A.S. Baird, K.M. Kross, D. Gottschalk, E.A. Hinson, N. Wood, K.A. Layman, Attenuated Total Reflection Fourier Transform Infrared Spectroscopic Investigation of CO Adsorption on Hydrated Ru/Al2O3, J. Phys. Chem. C. 111 (2007) 14207–14214. https://doi.org/10.1021/jp0733421.
[45] H. Yoshida, S. Narisawa, S. Fujita, L. Ruixia, M. Arai, In situ FTIR study on the formation and adsorption of CO on alumina-supported noble metal catalysts from H2 and CO2 in the presence of water vapor at high pressures, Phys. Chem. Chem. Phys. 14 (2012) 4724–4733. https://doi.org/10.1039/C2CP23590K.
[46] L.F. Bobadilla, A. Muñoz-Murillo, O.H. Laguna, M.A. Centeno, J.A. Odriozola, Does shaping catalysts modify active phase sites? A comprehensive in situ FTIR spectroscopic study on the performance of a model Ru/Al2O3 catalyst for the CO methanation, Chemical Engineering Journal. 357 (2019) 248–257. https://doi.org/10.1016/j.cej.2018.09.166.
[47] P. Dongapure, S. Bagchi, S. Mayadevi, R.N. Devi, Variations in activity of Ru/TiO2 and Ru/Al2O3 catalysts for CO2 hydrogenation: An investigation by in-situ infrared spectroscopy studies, Molecular Catalysis. 482 (2020) 110700. https://doi.org/10.1016/j.mcat.2019.110700.
[48] J.-M. Andanson, A. Baiker, Exploring catalytic solid/liquid interfaces by in situ attenuated total reflection infrared spectroscopy, Chem. Soc. Rev. 39 (2010) 4571–4584. https://doi.org/10.1039/B919544K.
[49] H. Ishikawa, J.N. Kondo, K. Domen, Hydrogen Adsorption on Ru/ZrO2 Studied by FT-IR, J. Phys. Chem. B. 103 (1999) 3229–3234. https://doi.org/10.1021/jp9842852.
[50] D.S. Rivera Rocabado, T.G. Noguchi, S. Hayashi, N. Maeda, M. Yamauchi, T. Ishimoto, Adsorption States of N2/H2 Activated on Ru Nanoparticles Uncovered by Modulation–Excitation Infrared Spectroscopy and Density Functional Theory Calculations, ACS Nano. 15 (2021) 20079–20086. https://doi.org/10.1021/acsnano.1c07825.
[51] D.S. Rivera Rocabado, M. Aizawa, T.G. Noguchi, M. Yamauchi, T. Ishimoto, Uncovering the Mechanism of the Hydrogen Poisoning on Ru Nanoparticles via Density Functional Theory Calculations, Catalysts. 12 (2022) 331. https://doi.org/10.3390/catal12030331.
[52] H. Ogasawara, M. Ito, Hydrogen adsorption on Pt(100), Pt(110), Pt(111) and Pt(1111) electrode surfaces studied by in situ infrared reflection absorption spectroscopy, Chemical Physics Letters. 221 (1994) 213–218. https://doi.org/10.1016/0009-2614(94)00247-9.